

# Turbulence and Shock-Waves in Crowd Dynamics

Vladimir G. Ivancevic and Darryn J. Reid  
 Land Operations Division  
 Defence Science & Technology Organisation

## Abstract

In this paper we analyze crowd turbulence from both classical and quantum perspective. We analyze various crowd waves and collisions using crowd macroscopic wave function. In particular, we will show that nonlinear Schrödinger (NLS) equation is fundamental for quantum turbulence, while its closed-form solutions include shock-waves, solitons and rogue waves, as well as planar de Broglie's waves. We start by modeling various crowd flows using classical fluid dynamics, based on Navier–Stokes equations. Then, we model turbulent crowd flows using quantum turbulence in Bose-Einstein condensation, based on modified NLS equation.

**Keywords:** Crowd behavior dynamics, classical and quantum turbulence, shock waves, solitons and rogue waves

## Contents

<b>1</b>	<b>Introduction</b>	<b>2</b>
<b>2</b>	<b>Classical Approach to Crowd Turbulence</b>	<b>4</b>
2.1	Classical Turbulence and Crowd Flows . . . . .	4
2.2	Navier-Stokes Crowd Fluids . . . . .	7
2.3	Isovorticial 2D Crowd Flows . . . . .	9
<b>3</b>	<b>Quantum Approach to Crowd Turbulence</b>	<b>12</b>
3.1	Quantum Turbulence . . . . .	12
3.2	Bose-Einstein Crowd Superfluids . . . . .	14
3.3	Kolmogorov Energy Spectra . . . . .	16
<b>4</b>	<b>A Variety of Crowd Waves</b>	<b>17</b>
4.1	Crowd Shock-Waves, Solitons and Rogue Waves . . . . .	17
4.2	Collision of Two Crowds . . . . .	19
4.3	Quantum Linear Crowd Waves . . . . .	20
<b>5</b>	<b>Conclusion</b>	<b>23</b>
<b>6</b>	<b>Appendix: Basic Lie Algebra Mechanics</b>	<b>23</b>

# 1 Introduction

Massive crowd movements can be today precisely observed from satellites. All that one can see is physical movement of the crowd. Therefore, all involved psychology of individual crowd agents (and their groups within the crowd): cognitive, motivational and emotional, as well as its global sociology, is only a non-transparent input (a hidden initial switch) to the fully observable crowd physics [1, 2, 3, 4]. About a decade ago, D. Helbing discovered a phenomenon called *crowd turbulence* (see [5, 6, 7, 8, 9]), depicting crowd disasters caused by the panic stampede that can occur at high pedestrian densities and which is a serious concern during various disasters (bushfires, tornados, earthquakes), as well as mass events like soccer championship games or annual pilgrimage in Mecca.

The adaptive, wave-form, nonlinear and stochastic crowd dynamics has been modeled using (an adaptive form of) *nonlinear Schrödinger equation*<sup>1</sup> (NLS), also called *Gross-Pitaevskii equation*<sup>2</sup> (GP), defining the time-dependent complex-valued *macroscopic wave function*  $\psi = \psi(x, t)$ , whose absolute square  $|\psi(x, t)|^2$  represents the *crowd density function*. In natural quantum units ( $\hbar = 1$ ,  $m = 1$ ), our NLS equation reads:

$$i\partial_t\psi = -\frac{1}{2}\partial_{xx}\psi + V|\psi|^2\psi, \quad (i = \sqrt{-1}; \quad \text{with } \partial_z\psi = \frac{\partial\psi}{\partial z}), \quad (1)$$

where  $V = V(w, x)$  denotes the adaptive heat potential (trained by either Hebbian or Levenberg-Marquardt learning). Physically, the NLS equation (1) describes a nonlinear wave in a quantum matter (such as Bose-Einstein condensates).

For general crowd simulation, we recently proposed two NLS-based approaches in [4], each representing a *quantum neural network* [10]:

**Weak coupling approach:** A looser (and more abstract) but higher-dimensional approach consisting of an  $n$ -dimensional set of NLS equations:

$$i\partial_t\psi_i = -\frac{1}{2}\partial_{xx}\psi_i + V|\psi_i|^2\psi_i, \quad (i = 1, \dots, n), \quad (2)$$

which self-organize in a common adaptive potential  $V = V(w, x)$ . Here, the squared amplitude  $|\psi|^2$  is the *condensate density*. The potential  $V(w, x)$  includes synaptic weights  $w_k$ ,

---

<sup>1</sup>The most important case of nonlinear Schrödinger equation is the *cubic NLS*

$$i\partial_t\psi = -\frac{1}{2}\Delta\psi \pm |\psi|^2\psi,$$

with the cubic nonlinearity  $|\psi|^2\psi$ . The sign  $+$  in the cubic NLS represents *defocusing NLS*, while the  $-$  sign represents *focusing NLS*. This extraordinarily rich nonlinear PDE represents a fully integrable Hamiltonian system which is traditionally studied on Euclidean domains  $\mathbb{R}^n$  (but other domains, like circle, torus or hypersphere, are also studied) – and allows for a ‘zoo’ of various wave-like solutions (to be analyzed later). Terms *sub-critical*, *critical*, and *super-critical* are frequently used to denote a significant transition in the behavior of a particular equation with respect to a specified regularity class (or conserved quantity). Typically, sub-critical equations behave in an approximately linear manner, supercritical equation behave in a highly nonlinear manner, and critical equations are very finely balanced between the two. Occasionally one also discusses the sub-criticality, criticality, or super-criticality of regularities with respect to other symmetries than scaling, such as Galilean invariance or Lorentz invariance. For survey of recent advances in nonlinear wave equations based on their criticality, see [12].

<sup>2</sup>NLS or GP is also similar in form to the Ginzburg-Landau equation, a mathematical theory used to model superconductivity.

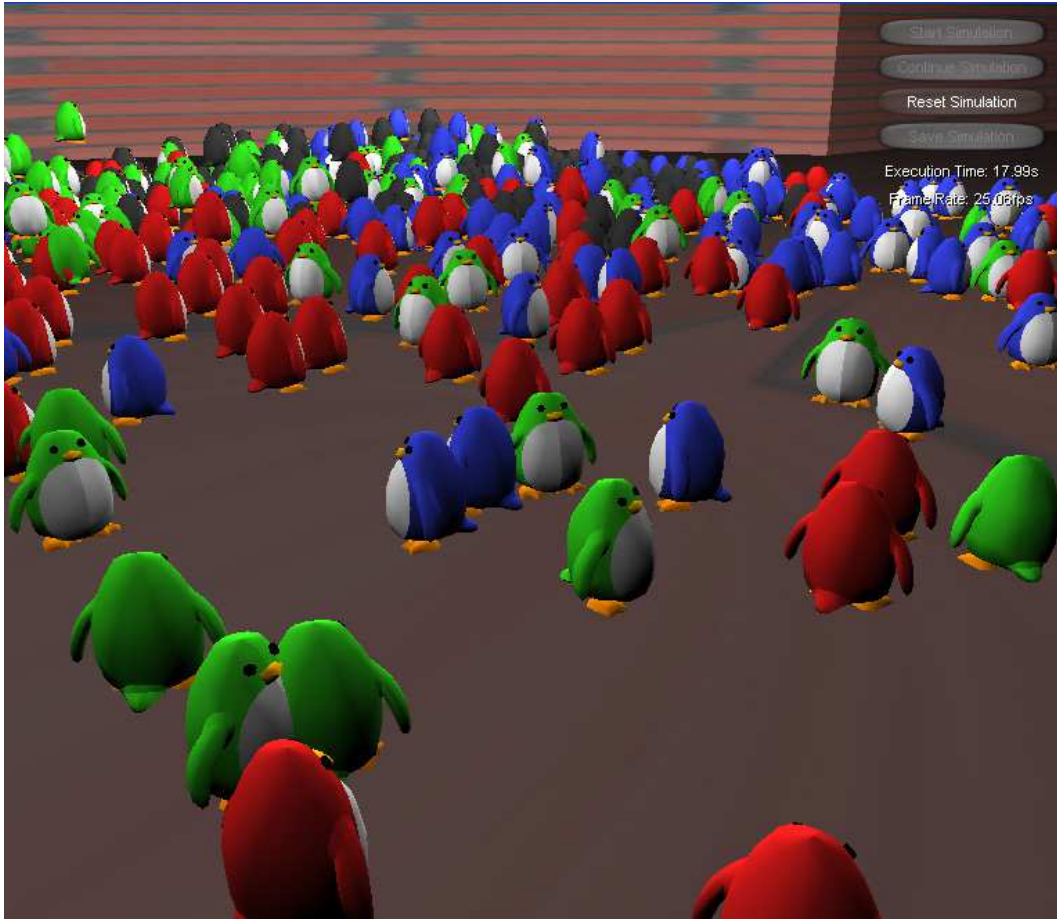


Figure 1: Simulating random-mixing behavior of four crowds in a confined environment.

which iteratively update according to the standard Hebbian rule:

$$\dot{w}_i = -w_i + c|\psi|g_i|\psi|, \quad V(w, x) = \sum_{i=1}^n w_i g_i,$$

where  $c$  is the learning rate parameter and  $g_i$  are Gaussian kernel functions with means  $x_i$  and standard deviations normalized to unity. The system (2) was numerically solved using the Method of Lines (combined with the fast adaptive Runge-Kutta-Fehlberg integrator with Cash-Karp accelerator). Its solution<sup>3</sup> represents time evolution in the complex plane  $\mathbb{C}$  of  $n$

---

<sup>3</sup>Crowd simulations were based on the following data:

1. Target function used for this case is:  $f = 2 \sin(20\pi t)$ . An infinitesimal tracking function used is:  $h = -(PDF \cdot dx/x)$ .
2. Gaussian kernel functions are defined as:  $g_i = \exp[-(v - m_i)^2]$ , where  $v = f - h$ , while  $m_i$  are random

cooperative groups, each consisting of  $m$  agents of  $SE(2)$ -kinematic type.<sup>4</sup> In this approach, each individual line (or kinematic trajectory), defines a velocity controller for a single agent. The total number of agents, as well as number of groups, is limited only by the available computation power.

**Strong coupling approach:** A pair of strongly-coupled NLS equations with Hebbian learning:

$$\begin{aligned}
\text{BLUE} & : \quad i\partial_t\psi_B = -\frac{a_B}{2}|\phi_R|^2\partial_{xx}\psi_B + V|\psi_B|^2\psi_B, \\
\text{RED} & : \quad i\partial_t\phi_R = -\frac{b_R}{2}|\psi_B|^2\partial_{xx}\phi_R + V|\phi_R|^2\phi_R, \\
\text{HEBB} & : \quad \dot{w}_i = -w_i + c_H|\psi_B|g_i|\phi_R|, \quad V = \sum_{i=1}^n w_i g_i.
\end{aligned} \tag{3}$$

Here,  $a_B, b_R, c_H$  are parameters related to Red, Blue and Hebb, equations respectively. This is a bidirectional, spatiotemporal, complex-valued associative memory machine, generalizing Lanchester and Lotka-Volterra predator-prey dynamical systems, as well as Hopfield, Kosko and Grossberg models of neural networks (see, e.g. [11]).

In this paper we will analyze crowd turbulence (from both classical and quantum perspective) as well as various crowd waves and collisions. In particular, we will show that NLS equation (1) is fundamental for quantum turbulence, while its closed-form solutions include shock-waves, solitons and rogue waves. Firstly, we will model various crowd flows using classical fluid dynamics, based on Navier–Stokes equations. Then, we will model turbulent crowd flows using quantum turbulence in Bose-Einstein condensation, based on modified NLS equation.

## 2 Classical Approach to Crowd Turbulence

In this section we model various crowd flows using models from classical fluid dynamics, based on Navier–Stokes partial differential equations (PDEs).

### 2.1 Classical Turbulence and Crowd Flows

Turbulence has long been one of the great mysteries in nature, with discussion dating back to the era of Leonardo da Vinci. He observed the turbulent flow of water and drew pictures showing

---

Gaussian means.

3. Potential field update is given by the scalar product:  $V_{i+1} = V_i + w_i \cdot g_i$ .
4. The complex plane  $\mathbb{C}$  was embedded in the 3D graphics environment (both urban and bush) with 3D collision dynamics.

<sup>4</sup>The Euclidean motion group  $SE(2) \equiv SO(2) \times \mathbb{R}$  is a set of all  $3 \times 3$ - matrices of the form:

$$\begin{bmatrix} \cos \theta & \sin \theta & x \\ -\sin \theta & \cos \theta & y \\ 0 & 0 & 1 \end{bmatrix},$$

including both rigid translations (i.e., Cartesian  $x, y$ -coordinates) and rotation matrix  $\begin{bmatrix} \cos \theta & \sin \theta \\ -\sin \theta & \cos \theta \end{bmatrix}$  in Euclidean plane  $\mathbb{R}^2 \approx \mathbb{C}$  (see [15, 16]).

that turbulence has a structure comprised of vortices of different sizes (Figure 2). After Leonardo, turbulence has been intensely studied in a number of fields, but it is still far from completely understood. This is primarily because turbulence is a strongly nonlinear dynamical phenomenon.



Figure 2: Sketch of turbulence by Leonardo da Vinci.

*Turbulent flow* is a fluid flow regime characterized by low momentum diffusion, high momentum convection, and rapid variation of pressure and velocity in space and time. Flow that is not turbulent is called *laminar flow*. Also, recall that the *Reynolds number*  $Re$  characterizes whether flow conditions lead to laminar or turbulent flow. The structure of turbulent flow was first described by A. Kolmogorov. Consider the flow of water over a simple smooth object, such as a sphere. At very low speeds the flow is laminar, i.e., the flow is locally smooth (though it may involve vortices on a large scale). As the speed increases, at some point the transition is made to turbulent (or, chaotic) flow. In turbulent flow, unsteady *vortices*<sup>5</sup> appear on many scales and interact with each

---

<sup>5</sup>Vortex can be any circular or rotary flow that possesses vorticity. Vortex represents a spiral whirling motion (i.e., a spinning turbulent flow) with closed streamlines. The shape of media or mass rotating rapidly around a center forms a vortex. It is a flow involving rotation about an arbitrary axis and can be described by the vector curl operator.

In the atmospheric sciences, vorticity is a property that characterizes large-scale rotation of air masses. Since the atmospheric circulation is nearly horizontal, the 3D vorticity is nearly vertical, and it is common to use the vertical component as a scalar vorticity.

A vortex can be seen in the spiraling motion of air or liquid around a center of rotation. Circular current of water of conflicting tides form vortex shapes. Turbulent flow makes many vortices. A good example of a vortex is the atmospheric phenomenon of a whirlwind or a *tornado*. This whirling air mass mostly takes the form of a helix, column, or spiral. Tornadoes develop from severe thunderstorms, usually spawned from squall lines and *supercell thunderstorms*, though they sometimes happen as a result of a *hurricane*. (A hurricane is a much larger, swirling body of clouds produced by evaporating warm ocean water and influenced by the Earth's rotation. In particular, polar vortex is a persistent, large-scale cyclone centered near the Earth's poles, in the middle and upper troposphere and the stratosphere. Similar, but far greater, vortices are also seen on other planets, such as the permanent Great Red Spot on Jupiter and the intermittent Great Dark Spot on Neptune.) Another example is a meso-vortex on the scale of a few miles (smaller than a hurricane but larger than a tornado). On a much smaller scale, a vortex

other. Drag due to boundary layer skin friction increases. The structure and location of boundary layer separation often changes, sometimes resulting in a reduction of overall drag.

Applied to crowd dynamics, *vorticity*  $\boldsymbol{\omega} = \boldsymbol{\omega}(\mathbf{x}, t)$  is defined as the circulation per unit area at a point in the crowd flow field, that is as the curl of the the crowd flow velocity:  $\boldsymbol{\omega} = \nabla \times \mathbf{u}$ . It is a vector quantity, whose direction is approximately along the axis of the swirl. The movement of a crowd flow can be said to be vortical if the fluid moves around in a circle, or in a helix, or if it tends to spin around some axis. Such motion can also be called *solenoidal*.

Because laminar–turbulent transition in crowd dynamics is governed by Reynolds number, the same transition occurs if the size of the crowd is gradually increased, or the viscosity of the crowd is decreased, or if the density of the crowd is increased.

In particular, in a turbulent crowd flow, there is a range of scales of the crowd flow motions, called *eddies*. A single packet of crowd flow moving with a bulk velocity is called an ‘eddy’. The size of the largest scales (eddies) are set by the overall geometry of the crowd flow.<sup>6</sup>

Such turbulent crowd flow shows characteristic statistical behavior (compare with [50, 51]). For simplicity, we will assume a steady state of fully developed turbulence of an incompressible classical crowd flow. Energy is injected into the crowd flow at a rate  $\varepsilon$  in an energy-containing range. In an inertial range, this crowd energy is transferred to smaller length scales without dissipation. In this range, the crowd is locally homogeneous and isotropic, leading to energy spectral statistics described by the *Kolmogorov law*,<sup>7</sup>

$$E(k) = C \varepsilon^{2/3} k^{-5/3}. \quad (4)$$

The crowd energy spectrum  $E(k)$  is defined by  $E = \int E(k) d\mathbf{k}$ , where  $E$  is the kinetic energy of the crowd per unit mass and  $k$  is the crowd wave-number from the Fourier transform of the velocity field (compare with the last subsection on quantum crowd waves). The spectrum of equation (4) is derived by assuming that  $E(k)$  is locally determined only by the crowd energy flux  $\varepsilon$  and by  $k$ . The crowd energy transferred to smaller scales is dissipated at the Kolmogorov wave-number  $k_K = (\varepsilon/\nu^3)^{1/4}$  in an energy-dissipative range via the viscosity of the crowd flow at a dissipation rate  $\varepsilon$  in equation (4), which is equal to the crowd energy flux  $\Phi$  in the inertial range. The Kolmogorov constant  $C$  is a dimensionless parameter of order unity. The inertial range is thought to be sustained by a self-similar *Richardson cascade* in which large crowd eddies break up into smaller eddies through crowd vortex reconnections.

In order for two crowd flows to be similar they must have the same geometry and equal Reynolds numbers. When comparing crowd flow behavior at homologous points in a crowd model and a full–

---

is usually formed as water goes down a drain, as in a sink or a toilet. This occurs in water as the revolving mass forms a whirlpool. (A whirlpool is a swirling body of water produced by ocean tides or by a hole underneath the vortex, where water drains out, as in a bathtub.) This whirlpool is caused by water flowing out of a small opening in the bottom of a basin or reservoir. This swirling flow structure within a region of fluid flow opens downward from the water surface. In the hydrodynamic interpretation of the behavior of electromagnetic fields, the acceleration of electric fluid in a particular direction creates a positive vortex of magnetic fluid. This in turn creates around itself a corresponding negative vortex of electric fluid.

<sup>6</sup>For comparison, in an industrial smoke-stack, the largest scales of fluid motion are as big as the diameter of the stack itself. The size of the smallest scales is set by  $Re$ . As  $Re$  increases, smaller and smaller scales of the flow are visible. In the smoke-stack, the smoke may appear to have many very small bumps or eddies, in addition to large bulky eddies. In this sense,  $Re$  is an indicator of the range of scales in the flow. The higher the Reynolds number, the greater the range of scales.

<sup>7</sup>The Kolmogorov spectrum has been confirmed experimentally and numerically in fluid turbulence at high Reynolds numbers.

scale crowd flow, we have  $Re^* = Re$ , where quantities marked with \* concern the flow around the crowd model and the other the real crowd flow.

## 2.2 Navier-Stokes Crowd Fluids

Fluid dynamicists believe that Navier–Stokes PDEs accurately describe turbulence (see, e.g. [49]). Therefore, we can assume that viscous crowd flows evolve according to nonlinear Navier–Stokes equations<sup>8</sup>

$$\dot{\mathbf{u}} + \mathbf{u} \cdot \nabla \mathbf{u} + \nabla p / \rho = \nu \Delta \mathbf{u} + \mathbf{f}, \quad (5)$$

where  $\mathbf{u} = \mathbf{u}(\mathbf{x}, t)$  is the 3D velocity of a crowd flow,  $\dot{\mathbf{u}} \equiv \partial_t \mathbf{u}$  is the 3D acceleration of a crowd flow,  $p = p(\mathbf{x}, t)$  is the crowd pressure field, while  $\mathbf{f} = \mathbf{f}(\mathbf{x}, t)$  is the external nonlinear energy source to the crowd, while  $\rho, \nu$  are the crowd flow density and viscosity coefficient, respectively. Such a crowd flow can be characterized by the ratio of the second term on the left-hand side of equation (5),  $\mathbf{u} \cdot \nabla \mathbf{u}$ , referred to as the crowd inertial term, and the second term on the right-hand side,  $\nu \Delta \mathbf{u}$ , that we call the crowd viscous term. This ratio defines the *Reynolds number*<sup>9</sup>  $Re = \bar{v} D / \nu$ , where  $\bar{v}$  and  $D$  are a characteristic velocity and length scale, respectively. When  $\bar{v}$  increases and the Reynolds number  $Re$  exceeds a critical value, the crowd changes from a *laminar* to a *turbulent* state, in which the crowd flow is complicated and contains eddies.<sup>10</sup> To simplify the problem, we can impose to  $\mathbf{f}$  the so-called *Reynolds condition*,  $\langle \mathbf{f} \cdot \mathbf{u} \rangle = \varepsilon$ , where  $\varepsilon$  is the average rate of energy injection.

In mechanical Lie algebra terms (see Appendix), the Navier–Stokes PDE (5) can be written:

$$\dot{\boldsymbol{\omega}} = -[\mathbf{u}, \boldsymbol{\omega}] + \text{curl } \mathbf{f} + \nu \Delta \boldsymbol{\omega}.$$

On the other hand, the *Euler equation* for ideal crowd flows,

$$\dot{\mathbf{u}} + \mathbf{u} \cdot \nabla \mathbf{u} + \nabla p / \rho = 0, \quad (6)$$

---

<sup>8</sup>Navier–Stokes equations, named after C.L. Navier and G.G. Stokes, are a set of PDEs that describe the motion of liquids and gases, based on the fact that changes in momentum of the particles of a fluid are the product of changes in pressure and dissipative viscous forces acting inside the fluid. These viscous forces originate in molecular interactions and dictate how viscous a fluid is, so the Navier–Stokes PDEs represent a dynamical statement of the balance of forces acting at any given region of the fluid. They describe the physics of a large number of phenomena of academic and economic interest (they are useful to model weather, ocean currents, water flow in a pipe, motion of stars inside a galaxy, flow around an airfoil (wing); they are also used in the design of aircraft and cars, the study of blood flow, the design of power stations, the analysis of the effects of pollution, etc).

<sup>9</sup>Reynold’s number  $Re$  is the most important dimensionless number in fluid dynamics and provides a criterion for determining *dynamical similarity*. Where two similar objects in perhaps different fluids with possibly different flow–rates have similar fluid flow around them, they are said to be dynamically similar.  $Re$  is the ratio of inertial forces to viscous forces and is used for determining whether a flow will be *laminar* or *turbulent*. Laminar flow occurs at low Reynolds numbers, where viscous forces are dominant, and is characterized by smooth, constant fluid motion, while turbulent flow, on the other hand, occurs at high  $Res$  and is dominated by inertial forces, producing random eddies, vortices and other flow fluctuations. The transition between laminar and turbulent flow is often indicated by a critical Reynold’s number ( $Re_{crit}$ ), which depends on the exact flow configuration and must be determined experimentally. Within a certain range around this point there is a region of gradual transition where the flow is neither fully laminar nor fully turbulent, and predictions of fluid behavior can be difficult.

<sup>10</sup>The first demonstration of the existence of an unstable recurrent pattern in a turbulent hydrodynamic flow was performed in [KK01], using the full numerical simulation, a 15,422–dimensional discretization of the 3D Plane Couette turbulence at the Reynold’s number  $Re = 400$ . The authors found an important unstable spatiotemporally–periodic solution, a single unstable recurrent pattern.

reads in Lie algebra terms,

$$\dot{\boldsymbol{\omega}} = -[\mathbf{u}, \boldsymbol{\omega}], \quad \boldsymbol{\omega} = \text{curl } \mathbf{u}.$$

Equation (6) is related to the Navier–Stokes PDE (5) in the same way as the classical Euler equation of a rigid body (with a fixed point, see Appendix),

$$\dot{\boldsymbol{\pi}} = \boldsymbol{\pi} \times \boldsymbol{\omega},$$

is associated to a more general equation, involving friction and external angular momentum [13, 14]

$$\dot{\boldsymbol{\pi}} = \boldsymbol{\pi} \times \boldsymbol{\omega} + \mathbf{F} - \nu \boldsymbol{\pi}, \quad (7)$$

the ‘friction operator’  $\nu$  is symmetric and positive definite. The distributed mass force  $\mathbf{f}$ , which appeared in the Navier–Stokes equation (5), is similar to the external angular momentum  $\mathbf{F}$ , and it is the origin of the crowd flow motion. The viscous friction  $\nu \Delta \mathbf{u}$  is analogous to the term  $-\nu \boldsymbol{\pi}$  in (7) slowing the rigid body motion. The similarity becomes especially noticeable if one rewrites the equations in components in the eigenbasis of the friction operator.

For example, for the Navier–Stokes equation with periodic boundary conditions one can expand the crowd vorticity field and the force  $\mathbf{f}$  into the ordinary Fourier series. The equations in both of the cases have the form of *Galerkin approximation*:

$$\dot{x}_i = \sum_{j,k} a_{ijk} x_j x_k + \sum_i f_i - \nu_i x_i. \quad (8)$$

The first term corresponds to the Euler equation (6) and describes the inertial crowd motion. It follows from the properties of (6) that the divergence of this term is equal to zero. Furthermore, the Euler equation of an ideal crowd flow in any dimension, as well as that of a rigid body, has a quadratic positive definite first integral, the kinetic energy. Therefore, for  $\mathbf{f} = \mathbf{u} = 0$ , the vector field on the right-hand side of (8) is tangent to certain ellipsoids centered at the crowd origin. This implies that during the crowd evolution defined by this equation there is neither growth nor decay of solutions.

The term  $-\nu_i x_i$  in (8), corresponding to the crowd friction, dominates over the constant ‘crowd pumping’  $\mathbf{f}$  when considered sufficiently far away from the crowd origin. Hence, in that remote crowd region, the crowd motion is directed towards the origin, and an infinite growth of solutions is impossible. Also, since the ‘crowd pumping’  $\mathbf{f}$  pushes a phase point out of any neighborhood of the origin, while the friction returns it from a distance, crowd motion in the system of a rigid body (7) approaches an intermediate regime-attractor. For instance, this crowd attractor can be a stable stagnation point or a periodic crowd motion, while for sufficiently high dimension of the phase space it can appear to be a *chaotic motion* sensitive to the initial conditions.

Here we recall that *chaos theory*, of which turbulence is the most extreme form, started in 1963, when E. Lorenz from MIT took the Navier–Stokes PDEs (5) and reduced them into three first-order coupled nonlinear ODEs, to demonstrate the idea of sensitive dependence upon initial conditions and associated *chaotic behavior*. The 3D *phase-portrait* of the Lorenz system (9) shows the celebrated ‘*Lorenz mask*’, a special type of *fractal attractor*.<sup>11</sup>

<sup>11</sup>The Lorenz reduced system of nonlinear ODEs

$$\dot{x} = a(y - x), \quad \dot{y} = bx - y - xz, \quad \dot{z} = xy - cz, \quad (9)$$

where  $x$ ,  $y$  and  $z$  are dynamical variables, constituting the 3D *phase-space* of the *Lorenz flow*; and  $a$ ,  $b$  and  $c$



If the crowd friction (or viscosity) coefficient  $\nu$  is high enough, then the crowd attractor will necessarily be a stable equilibrium position. While the parameter  $\nu$  decreases (i.e., the reciprocal parameter, the Reynolds number  $Re = 1/\nu$ , increases), bifurcations of the crowd equilibrium are possible, and the crowd attractor can become a periodic motion and later a totally ‘stochastic’ one.<sup>12</sup>

### 2.3 Isovorticial 2D Crowd Flows

Crowd 2D flow differs sharply from crowd 3D flow. According to V. Arnold, in the realm of fluid dynamics, the essence of this difference is contained in the difference in the geometries of the orbits of the co-adjoint representation (see Appendix) in the two and 3D cases [13, 14]. The character of the first, inertia, term in the Galerkin approximation (8) (of the Navier-Stokes PDEs (5)) changes drastically in the passage from 2D crowd flow flows to three- (or higher-) dimensional ones. The reason lies in the distinctions among the geometries of the coadjoint orbits of the corresponding diffeomorphism groups. In other words, in the 2D case the orbits are in some sense closed and behave like a family of level sets of a function. In the 3D case the orbits are more complicated; in particular, they are unbounded (and perhaps dense). The orbits of the coadjoint representation of the group of diffeomorphisms of a 3D Riemannian manifold can be described in the following way. Let  $v_1$  and  $v_2$  be two vector fields of velocities of a non-compressible crowd flow in the region

---

are the parameters of the system. Originally, Lorenz used this model to describe the unpredictable behavior of the weather, where  $x$  is the rate of convective overturning (convection is the process by which heat is transferred by a moving fluid),  $y$  is the horizontal temperature overturning, and  $z$  is the vertical temperature overturning; the parameters are:  $a \equiv P$ —proportional to the Prandtl number (ratio of the fluid viscosity of a substance to its thermal conductivity, usually set at 10),  $b \equiv R$ —proportional to the Rayleigh number (difference in temperature between the top and bottom of the system, usually set at 28), and  $c \equiv K$ —a number proportional to the physical proportions of the region under consideration (width to height ratio of the box which holds the system, usually set at 8/3). The Lorenz system (9) has the properties: (i) *symmetry*:  $(x, y, z) \rightarrow (-x, -y, z)$  for all values of the parameters, and (ii) the  $z$ -axis ( $x = y = 0$ ) is *invariant* (i.e., all trajectories that start on it also end on it).

Today, it is well-known that the Lorenz model is a paradigm for low-dimensional chaos in dynamical systems and this model or its modifications are widely investigated in connection with modelling purposes in meteorology, hydrodynamics, laser physics, superconductivity, electronics, oil industry, chemical and biological kinetics, etc.

The *Lorenz mask* (3D chaotic attractor) has the following characteristics: (i) trajectory does not intersect itself in three dimensions; (ii) trajectory is not periodic or transient; (iii) general form of the shape does not depend on initial conditions; and (iv) exact sequence of loops is very sensitive to the initial conditions.

<sup>12</sup>The hypothesis that this mechanism is responsible for the phenomenon of turbulenzation of a fluid motion for large Reynolds numbers has been suggested by many authors. In particular, to normalize the attractor, A.N. Kolmogorov suggested in 1965 considering the ‘pumping’ proportional to the same small parameter  $\nu$  as viscosity, and he formulated the following two conjectures [14]:

1. The weak conjecture: The maximum of the dimensions of minimal attractors (attractor is called a minimal attractor if it does not contain smaller attractors) in the phase space of the Navier-Stokes PDEs (5) (as well as of their Galerkin approximations (8)) grows along with the Reynolds number  $Re = 1/\nu$ .
2. The strong conjecture: Not only maximum, but also the minimum of the dimensions of the minimal attractors mentioned above increases with the Reynolds number  $Re$ . As far as we know, both of these hypotheses still remain open.

For the Lorenz system, the role of energy is played by a nonhomogeneous quadratic function. The instability in the Lorenz model is apparently stronger than in the Kolmogorov one. One can check how the motion along the Lorenz strange attractor sensitively depends on the initial conditions, while for the Kolmogorov model it remains a conjecture. It is proven only that a stationary flow indeed loses stability as the Reynolds number  $Re$  increases.

In 1970 Ruelle and Takens formulated the conjecture that turbulence is the appearance of attractors with sensitive dependence of motion on the initial conditions along them in the phase space of the Navier-Stokes equation [17].

$D$ . We say that the fields  $v_1$  and  $v_2$  are isovorticial if there is volume-preserving diffeomorphism  $g : D \rightarrow D$  which carries every closed contour  $\gamma$  in  $D$  to a new contour such that the circulation of the first field along the original contour is equal to the circulation of the second field along the new contour:

$$\oint_{\gamma} v_1 = \oint_{g\gamma} v_2$$

The image of an orbit of the co-adjoint representation in a Lie algebra is the set of vector fields isovorticial to the given vector field. We have the following law of conservation of circulation [13, 14]: The circulation of a field of velocities of an ideal crowd flow over a closed flow contour does not change when the contour is carried by the flow to a new position.

Now, for simplicity, we will assume that the region  $D$  of the crowd flow is 2D and oriented. The metric and orientation give a symplectic structure on  $D$ ; the field of crowd velocities has divergence zero and is therefore Hamiltonian. Therefore, this vector field is given by a Hamiltonian function (many-valued, in general, if the region  $D$  is not simply-connected). The Hamiltonian function of a field of crowd velocities is called the *stream-function*, and is denoted by  $\psi$ . Thus we have:

$$v = I \text{ grad } \psi,$$

where  $I$  is the operator of clockwise rotation by  $90^\circ$ .

The stream function of the commutator of two crowd vector fields turns out to be the Jacobian (or the Poisson bracket of Hamiltonian formalism) of the crowd stream functions of the original vector fields:

$$\psi_{[v_1, v_2]} = J(\psi_1, \psi_2).$$

The vorticity (or curl) of a 2D crowd field of velocities is the scalar function  $r$  such that the integral around any oriented crowd region  $\sigma$  in  $D$  of the product of  $r$  with the oriented area element is equal to the circulation of the field of crowd velocities around the boundary of  $\sigma$ :

$$\int_{\sigma} r dS = \oint_{\partial\sigma} v.$$

The crowd vorticity can be now computed in terms of the crowd stream function as:

$$r = -\Delta\psi.$$

In the simply-connected 2D case, isovorticity of crowd vector fields  $v_1$  and  $v_2$  means that the functions  $r_1$  and  $r_2$  (the vorticities of these fields) are carried to one another under a suitable volume-preserving diffeomorphism. Therefore, if two vector fields are in the image of the same orbit of the co-adjoint representation, then a whole series of functionals are equal. For example, the integrals of all powers  $k$  of the crowd vorticity are:

$$\int_D r_1^k dS = \int_D r_2^k dS.$$

In particular, Euler's equations of motion of a 2D ideal crowd flow:

$$\partial_t v + v \nabla v = -\nabla p, \quad \text{div } v = 0,$$

have an infinite collection of first integrals. For example, such a first integral is the integral of any power  $k$  of the crowd vorticity of the field of crowd velocities:

$$I_k = \iint_D (\partial_x v_2 - \partial_x v_1)^k dx \wedge dy,$$

where  $\wedge$  denotes the antisymmetric wedge product.

Following V. Arnold [13, 14], we obtain in this way the following assertions regarding stability of planar stationary crowd flows:

1. A stationary flow of an ideal crowd flow is distinguished from all crowd flows isovorticial to it by the fact that it is a conditional extremum (or critical point) of the crowd kinetic energy.
2. If (i) the indicated critical point is actually an extremum, i.e., a local conditional maximum or minimum, (ii) it satisfies certain (generally satisfied) regularity conditions, and (iii) the extremum is non-degenerate (the second differential is positive- or negative-definite), then the stationary crowd flow is stable (i.e., is a Lyapunov stable equilibrium position of Euler's equation).
3. The formula for the second differential of the crowd kinetic energy, on the tangent space to the manifold of crowd fields which are isovorticial to a given one, has the following form in the 2D case. Let  $D$  be a region in the Euclidean plane with cartesian coordinates  $x$  and  $y$ . Consider a stationary crowd flow with stream function  $\psi = \psi(x, y)$ . Then we have the quadratic crowd energy form  $d^2H$ , given by

$$d^2H = \frac{1}{2} \iint_D (\delta v)^2 + (\Delta\psi/\nabla\Delta\psi)(\delta r)^2 dx dy,$$

where  $\delta v$  is the variation of the field of crowd velocities (i.e., a vector of the tangent space indicated above), and  $\delta r = \text{curl } \delta v$ . We remark here that for a crowd stationary flow, the gradient vectors of the crowd stream function and its Laplacian are collinear. Therefore the ratio  $\Delta\psi/\nabla\Delta\psi$  makes sense. Furthermore, in a neighborhood of every point where the gradient of the crowd vorticity is not zero, the crowd stream function is a function of the vorticity function.

The above assertions lead to the conclusion that the positive or negative definiteness<sup>13</sup> of the quadratic crowd energy form  $d^2H$  is a sufficient condition for stability of the stationary crowd flow under consideration. The analogous proposition in the linearized fluid dynamics problem is called Rayleigh's theorem.

Now, consider  $N$  crowd vortices with velocity circulations  $k_i$ , ( $i = 1, \dots, N$ ) around them in the Euclidean plane  $\mathbb{R}^2$ . Then the crowd vorticity at any moment will be concentrated at  $N$  points, and the crowd circulations at each of them will remain constant forever. It is convenient to write the evolution of crowd vortices as a dynamical system in the crowd configuration space for the  $N$ -vortex

---

<sup>13</sup>A definite bilinear form is a bilinear form  $B(x, x)$  over some vector space  $V$  such that the associated quadratic form  $Q(x) = B(x, x)$  is definite, that is, has a real value with the same sign (positive or negative) for all non-zero  $x$ . According to that sign,  $B$  is called positive definite or negative definite. If  $Q(x)$  takes both positive and negative values, the bilinear form  $B(x, x)$  is called indefinite. If  $B(x, x) \geq 0$  for all  $x$ , then  $B$  is said to be positive semidefinite. Negative semidefinite bilinear forms are defined similarly.

system, the space  $\mathbb{R}^{2N}$  with coordinates  $z_i = (x_i, y_i)$  and symplectic structure  $\sum_i k_i dy_i \wedge dx_i$ . Then the crowd vortex evolution in  $\mathbb{R}^{2N}$  will be given by the following Kirchhoff–Hamiltonian system [18]:

$$k_i \dot{x}_i = \partial_{y_i} H, \quad k_i \dot{y}_i = -\partial_{x_i} H.$$

### 3 Quantum Approach to Crowd Turbulence

In this section we model turbulent crowd flows using models of quantum turbulence in Bose-Einstein condensation, based on modified nonlinear Schrödinger equation. Here, we want to go beyond classical turbulence as described in the previous section using Navier-Stokes equations. Essentially, we want to achieve two things here: (i) to provide a cleaner (more controllable and repetitive) simulation environment for crowd turbulence; and (ii) the ability to include into this environment a variety of nonlinear waves (e.g., shock-waves, solitons, breathers, rogue waves). From the physical perspective, the so-called ‘Bose-Einstein condensate’ will be our macroscopic quantum crowd superfluid model.

#### 3.1 Quantum Turbulence

Quantum turbulence was discovered in superfluid helium ( $^4\text{He}$ ) in the 1950s, but the field moved in a new direction starting around the mid 1990s (see [19, 20]). Briefly, quantum turbulence (see Figure 3) is comprised of quantized vortices that are definite topological defects arising from the order parameter appearing in *Bose-Einstein condensation* (BEC).<sup>14</sup> Hence quantum turbulence is expected to yield a simpler model of turbulence than does classical turbulence based on the Navier–Stokes PDE (5).

Bose-Einstein condensation is often considered to be a *macroscopic quantum phenomenon* (see, e.g. [21]). This is because bosons occupy the same single-particle ground state below a critical temperature through Bose-Einstein condensation to form a *macroscopic wave function* (order parameter) extending over the entire system. As a direct result of the formation of a macroscopic wave function, quantized vortices appear in the Bose-condensed system. A *quantized vortex*<sup>15</sup> is a vortex of inviscid superflow, and any rotational motion of a superfluid is sustained by quantized vortices. A quantized vortex is stable and well-defined topological defect, very different from classical vortices in a conventional fluid. Hydrodynamics dominated by quantized vortices is called *quantum superfluid dynamics*, and turbulence comprised of quantized vortices is known as *quantum turbulence* (QT) [19, 20].

Liquid  $^4\text{He}$  enters a superfluid state below the  $\lambda$  point ( $T_\lambda = 2.17$  K) with Bose–Einstein condensation of the  $^4\text{He}$  atoms.<sup>16</sup> The  $\lambda$  transition is closely related to the Bose-Einstein condensation

---

<sup>14</sup>A Bose–Einstein condensate (BEC) is a state of matter of a dilute gas of weakly interacting bosons confined in an external potential and cooled to temperatures very near absolute zero. It is the most common example of *quantum media*.

<sup>15</sup>The studies of quantized vortices originally began in 1950s using superfluid  $^4\text{He}$ , and much theoretical, numerical, and experimental effort has been devoted to the field. Superfluid  $^3\text{He}$ , discovered in 1972, presented a system with a variety of quantized vortices characteristic of p-wave superfluids.

<sup>16</sup>The characteristic phenomena of superfluidity were experimentally discovered in the 1930s by L. Kapitza [22] and Allen *et al.*[23]. The hydrodynamics of superfluid helium are well described by the two-fluid model proposed by Landau [24] and Tisza [25]. According to the two-fluid model, the system consists of an inviscid superfluid (density  $\rho_s$ ) and a viscous normal fluid (density  $\rho_n$ ) with two independent velocity fields  $\mathbf{v}_s$  and  $\mathbf{v}_n$ . The mixing ratio of the two fluids depends on the temperature. As the temperature is reduced below the  $\lambda$  point, the ratio of the superfluid

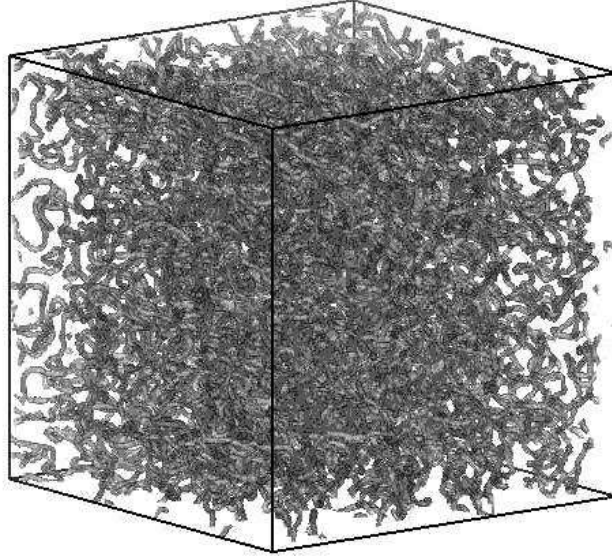


Figure 3: Quantum turbulence (QT) in Bose-Einstein condensation (BEC).

of  $^4\text{He}$  atoms, as first proposed by [27]. The Bose-condensed system exhibits the macroscopic wavefunction  $\psi(\mathbf{x}, t) = |\psi(\mathbf{x}, t)|e^{i\theta(\mathbf{x}, t)}$  as an order parameter. The superfluid velocity field is given by  $\mathbf{v}_x = (\hbar/m)\nabla\theta$ , with boson mass  $m$ , representing the potential flow. Since the macroscopic wave function should be single-valued for the space coordinate  $\mathbf{x}$ , the circulation  $\Gamma = \oint \mathbf{v} \cdot d\ell$  for an arbitrary closed loop in the fluid is quantized by the quantum  $\kappa = h/m$ . A vortex with quantized circulation is called a quantized vortex. Any rotational motion of a superfluid is sustained only by quantized vortices.<sup>17</sup>

The idea of quantized circulation was first proposed by L. Onsager, for a series of annular rings in a rotating superfluid [28]. R. Feynman considered that a vortex in a superfluid could take the form of a vortex filament, with the quantized circulation  $\kappa$  and a core of atomic dimension [29].<sup>18</sup> Vinen

---

component increases, and the fluid becomes entirely superfluid below about 1 K. The two-fluid model successfully explained the phenomena of superfluidity, while it was known in 1940s that superfluidity breaks down when it flows fast [26] and this phenomenon was not explained through the two-fluid model. This was later found to be caused by turbulence of the superfluid component due to random motion of quantized vortices.

<sup>17</sup>A quantized vortex is a topological defect characteristic of a Bose–Einstein condensate, and is different from a vortex in a classical viscous fluid. First, the circulation is quantized, which is contrary to a classical vortex that can have any circulation value. Second, a quantized vortex is a vortex of inviscid superflow. Thus, it cannot decay by the viscous diffusion of vorticity that occurs in a classical fluid. Third, the core of a quantized vortex is very thin, of the order of the coherence length, which is only a few angstroms in superfluid  $^4\text{He}$ . Because the vortex core is very thin and does not decay by diffusion, it is always possible to identify the position of a quantized vortex in the fluid. These properties make a quantized vortex more stable and definite than a classical vortex.

<sup>18</sup>Early experimental studies on superfluid hydrodynamics focused primarily on thermal counterflow. The flow is

confirmed Feynman’s findings experimentally, by showing that the dissipation arises from mutual friction between vortices and the normal flow [32, 33, 34, 35]. Vinen also succeeded in observing quantized circulation using vibrating wires in rotating superfluid  $^4\text{He}$  [36]. Subsequently, many experimental studies have examined *superfluid turbulence* (ST) in thermal counterflow systems, and have revealed a variety of physical phenomena [37]. Since the dynamics of quantized vortices are nonlinear and non-local, it has not been easy to quantitatively understand these observations on the basis of vortex dynamics. Schwarz clarified the picture of ST based on tangled vortices by numerical simulation of the quantized vortex filament model in the thermal counterflow [38, 39]. However, since the thermal counterflow has no analogy in conventional fluid dynamics, this study was not helpful in clarifying the relationship between ST and *classical turbulence* (CT). Superfluid turbulence is often called quantum turbulence (QT), which emphasizes the belief that it is comprised of quantized vortices [19, 20].

### 3.2 Bose-Einstein Crowd Superfluids

Recall from the first section, what happens if we rotate a cylindrical vessel with a classical viscous fluid inside. Even if the fluid is initially at rest, it starts to rotate and eventually reaches a steady rotation with the same rotational speed as the vessel. In that case, one can say that the system contains a vortex that mimics solid-body rotation. A rotation of arbitrary angular velocity can be sustained by a single vortex.

However, this does not occur in a *quantum superfluid*. Because of quantization of circulation, *superfluids* respond to rotation, not with a single vortex, but with a *lattice of quantized vortices*. R. Feynman noted that in uniform rotation with angular velocity  $\Omega$  the curl of the superfluid velocity is the circulation per unit area, and since the curl is  $2\Omega$ , a lattice of quantized vortices with number density  $n_0 = \text{curl } v_x / \kappa = 2\Omega / \kappa$  (the ‘Feynman rule’) arranges itself parallel to the rotation axis [29]. Such experiments were performed for superfluid  $^4\text{He}$ : Packard *et al.* visualized vortex lattices on the rotational axis by trapping electrons along the cores [40, 41]. This idea has also been applied to atomic Bose-Einstein condensates. Several groups have observed vortex lattices in rotating BECs<sup>19</sup> [43, 44, 45, 42].

This observation has been reproduced by a simulation of the Gross-Pitaevskii (GP) equation for the *macroscopic wave-function*  $\psi(\mathbf{x}, t) = |\psi(\mathbf{x}, t)|e^{i\theta(\mathbf{x}, t)}$  in 2D [46, 47] and 3D [48] spaces. In a weakly interacting Bose system, the macroscopic wave-function  $\psi(\mathbf{x}, t)$  appears as the order parameter of the Bose-Einstein condensate (representing our quantum crowd superfluid model)

---

driven by an injected heat current, and the normal fluid and superfluid flow in opposite directions. The superflow was found to become dissipative when the relative velocity between the two fluids exceeds a critical value [26]. Gorter and Mellink attributed the dissipation to mutual friction between two fluids, and considered the possibility of superfluid turbulence. Feynman proposed a turbulent superfluid state consisting of a tangle of quantized vortices [29]. Hall and Vinen performed the experiments of second sound attenuation in rotating  $^4\text{He}$ , and found that the mutual friction arises from interaction between the normal fluid and quantized vortices [30, 31]; second sound refers to entropy wave in which superfluid and normal fluid oscillate oppositely, and its propagation and attenuation give the information of the vortex density in the fluid.

<sup>19</sup>Among them, Madison *et al.* directly observed nonlinear processes such as vortex nucleation and lattice formation in a rotating  $^{87}\text{Rb}$  BEC [45]. By sudden application of a rotation along the trapping potential, an initially axi-symmetric condensate undergoes a collective quadrupole oscillation to an elliptically deformed condensate. This oscillation continues for a few hundred milliseconds with gradually decreasing amplitude. Then the axial symmetry of the condensate is recovered and vortices enter the condensate through its surface, eventually settling into a lattice configuration.

obeying the GP equation, or the modified cubic NLS equation (extended by the linear term  $-\mu\psi$ ):

$$i\hbar\partial_t\psi = -\frac{\hbar^2}{2m}\Delta\psi + V|\psi|^2\psi - \mu\psi. \quad (10)$$

Writing  $\psi = |\psi|\exp(i\theta)$ , the squared amplitude  $|\psi|^2$  is the *crowd superfluid density* and the gradient of the phase  $\theta$  gives the *crowd superfluid velocity*  $\mathbf{v}_x = (\hbar/m)\nabla\theta$ , corresponding to frictionless flow of the crowd. This relation causes quantized vortices to appear with quantized crowd circulation. The only characteristic scale of the GP model is the coherence length defined by  $\xi = \hbar/(\sqrt{2mV}|\psi|)$ , which determines the crowd vortex core size. The GP model can explain not only the crowd vortex dynamics but also phenomena related to vortex cores, such as crowd reconnection and nucleation.

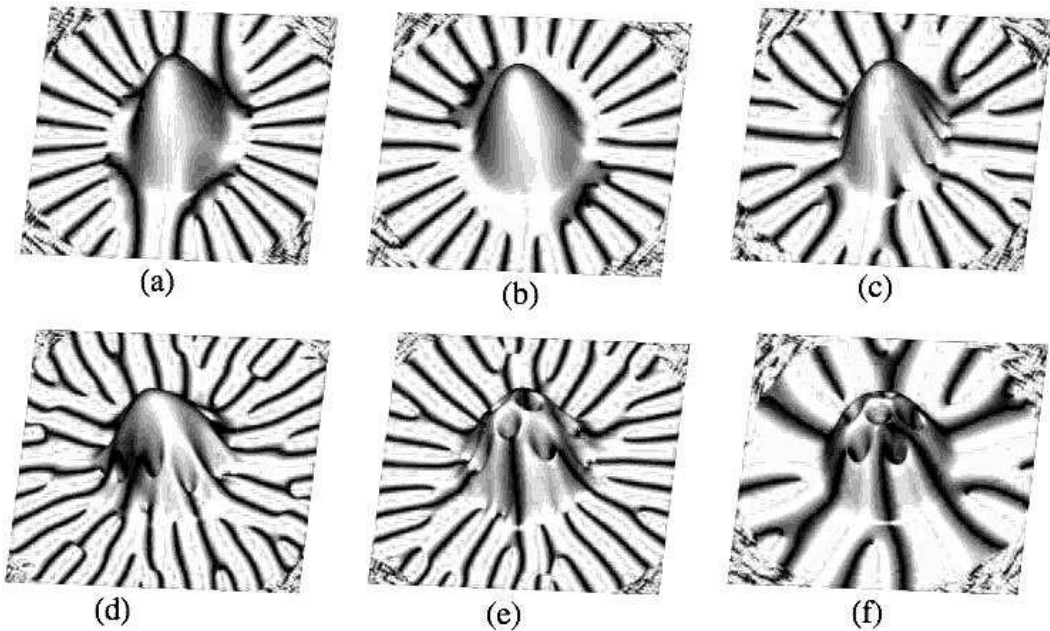


Figure 4: A typical crowd vortex lattice formation (modified and adapted from [19]).

A typical 2D numerical simulation of equation (10) (adapted from [46, 47]) for the crowd vortex lattice formation is shown in Figure 4, where the crowd superfluid density and the phase are displayed together. The trapping potential is

$$V_{\text{ex}} = \frac{1}{2}m\omega^2[(1 + \epsilon_x)x^2 + (1 + \epsilon_y)y^2],$$

where  $\omega = 2\pi \times 219$  Hz, and the parameters  $\epsilon_x$  and  $\epsilon_y$  describe small deviations from axisymmetry corresponding to experiments [44, 45]. Following [19, 20], we first prepare an equilibrium condensate trapped in a stationary potential; the size of the condensate cloud is determined by the Thomas-Fermi radius  $R_{\text{TF}}$ . When we apply a rotation with  $\Omega = 0.7\omega$ , the condensate becomes elliptic and performs a quadrupole oscillation [Fig. 4(a)]. Then, the boundary surface of the condensate becomes unstable and generates ripples that propagate along the surface [Fig. 4(b)]. As

stated previously, it is possible to identify quantized vortices in the phase profile also. As soon as the rotation starts, many vortices appear in the low-density region outside of the condensate [Fig. 4(a)]. Since quantized vortices are excitations, their nucleation increases the energy of the system. Because of the low density in the outskirts of the condensate, however, their nucleation contributes little to the energy and angular momentum.<sup>20</sup> Since these vortices outside of the condensate are not observed in the density profile, they are called ‘ghost vortices’. Their movement toward the Thomas-Fermi surface excites ripples [Fig. 4(b)]. It is not easy for these ghost vortices to enter the condensate, because that would increase both the energy and angular momentum. Only some vortices enter the condensate cloud to become ‘real vortices’ wearing the usual density profile of quantized vortices [Fig. 4(d)], eventually forming a vortex lattice [Fig. 4(e) and (f)]. The number of vortices forming a lattice is given by ‘Feynman’s rule’  $n_0 = 2\Omega/\kappa$ . The numerical results agree quantitatively with these observations. Here we remark on the essence of nonlinear dynamics. The initial state has no vortices in the absence of rotation. The final state is a vortex lattice corresponding to rotational frequency  $\Omega$ . In order to go from the initial to the final state, the system makes use of as many excitations as possible, such as vortices, quadruple oscillation, and surface waves. These experimental and theoretical results demonstrate typical behavior of quantum fluid dynamics in atomic BECs [19, 20].

### 3.3 Kolmogorov Energy Spectra

The Kolmogorov energy spectra were confirmed for both decaying [54] and steady [55] QT by the GP model. The normalized GP equation is:

$$i\partial_t\psi = -\frac{1}{2}\Delta\psi + V|\psi|^2\psi - \mu\psi, \quad (11)$$

which determines the dynamics of the macroscopic wave-function  $\psi(\mathbf{x}, t) = f(\mathbf{x}, t) \exp[i\phi(\mathbf{x}, t)]$ . The crowd superfluid dynamics in the GP model are compressible. The total number of crowd agents is  $N = \int |\psi|^2 d\mathbf{x}$  and the total crowd energy is:

$$E(t) = \frac{1}{N} \int^* \psi \left( -\Delta + \frac{V}{2} f^2 \right) \psi d\mathbf{x},$$

as represented by the sum of the interaction energy  $E_{int}(t)$ , the quantum energy  $E_q(t)$ , and the kinetic energy  $E_{kin}(t)$  [56, 57],

$$E_{int}(t) = \frac{V}{2N} \int f^4 d\mathbf{x}, \quad E_q(t) = \frac{1}{N} \int [\nabla f]^2 d\mathbf{x}, \quad E_{kin}(t) = \frac{1}{N} \int [f\nabla\phi]^2 d\mathbf{x}.$$

The kinetic energy is further divided into a compressible part  $E_{kin}^c(t)$  due to compressible excitations and an incompressible part  $E_{kin}^i(t)$  due to vortices. The Kolmogorov spectrum is expected for  $E_{kin}^i(t)$ <sup>21</sup> [19, 20].

<sup>20</sup>Actually the vortex-antivortex pairs are nucleated in the low-density region. Then the vortices parallel to the rotation are dragged into the Thomas-Fermi surface, while the antivortices are repelled to the outskirts.

<sup>21</sup>The failure to obtain a Kolmogorov law in the pure GP model [56, 57] is attributable to the following (see [19, 20]). The simulations showed that  $E_{kin}^i(t)$  decreases and  $E_{kin}^c(t)$  increases while the total energy  $E(t)$  is conserved because many compressible excitations are created through vortex reconnections [52, 53] and disturb the Richardson cascade of quantized vortices. Kobayashi *et al.* overcame these difficulties and obtained a Kolmogorov



## 4 A Variety of Crowd Waves

### 4.1 Crowd Shock-Waves, Solitons and Rogue Waves

The general crowd NLS equation (1) was exactly solved in [60, 61, 58] using the power series expansion method of Jacobi elliptic functions [62]. Consider the  $\psi$ -function describing a single plane wave, with the wave number  $k$  and circular frequency  $\omega$ :

$$\psi(x, t) = \phi(\xi) e^{i(kx - \omega t)}, \quad \text{with } \xi = x - kt \text{ and } \phi(\xi) \in \mathbb{R}. \quad (12)$$

Its substitution into the NLS equation (1) gives the nonlinear crowd oscillator ODE:

$$\phi''(\xi) + [\omega - \frac{1}{2}k^2] \phi(\xi) - V\phi^3(\xi) = 0. \quad (13)$$

We can seek a solution  $\phi(\xi)$  for (13) as a linear function [61]

$$\phi(\xi) = a_0 + a_1 \text{sn}(\xi),$$

where  $\text{sn}(x) = \text{sn}(x, m)$  are Jacobi elliptic sine functions with *elliptic modulus*  $m \in [0, 1]$ , such that  $\text{sn}(x, 0) = \sin(x)$  and  $\text{sn}(x, 1) = \tanh(x)$ . The solution of (13) was calculated in [58] to be

$$\begin{aligned} \phi(\xi) &= \pm m \sqrt{\frac{1}{V}} \text{sn}(\xi), & \text{for } m \in [0, 1]; \text{ and} \\ \phi(\xi) &= \pm \sqrt{\frac{1}{V}} \tanh(\xi), & \text{for } m = 1. \end{aligned}$$

This gives the exact periodic solution of (1) as [58]

$$\psi_1(x, t) = \pm m \sqrt{\frac{1}{V(w)}} \text{sn}(x - kt) e^{i[kx - \frac{1}{2}t(1+m^2+k^2)]}, \quad \text{for } m \in [0, 1]; \quad (14)$$

$$\psi_2(x, t) = \pm \sqrt{\frac{1}{V(w)}} \tanh(x - kt) e^{i[kx - \frac{1}{2}t(2+k^2)]}, \quad \text{for } m = 1, \quad (15)$$

where (14) defines the general solution, while (15) defines the *crowd envelope shock-wave*<sup>22</sup> (or, ‘dark soliton’) solution of the crowd NLS equation (1).

---

spectrum in QT that revealed an energy cascade [54, 55]. By performing numerical calculations of the Fourier-transformed GP equation with dissipation, they confirmed the Kolmogorov spectra for decaying turbulence [54]. To obtain a turbulent state, they started the calculation from an initial configuration in which the density was uniform and the phase of the wave-function had a random spatial distribution. The initial state was dynamically unstable and soon developed turbulence with many vortex loops. The spectrum  $E_{kin}^i(k, t)$  was then found to obey the Kolmogorov law.

<sup>22</sup>A shock wave is a type of fast-propagating nonlinear disturbance that carries energy and can propagate through a medium (or, field). It is characterized by an abrupt, nearly discontinuous change in the characteristics of the medium. The energy of a shock wave dissipates relatively quickly with distance and its entropy increases. On the other hand, a soliton is a self-reinforcing nonlinear solitary wave packet that maintains its shape while it travels at constant speed. It is caused by a cancelation of nonlinear and dispersive effects in the medium (or, field).

Alternatively, if we seek a solution  $\phi(\xi)$  as a linear function of Jacobi elliptic cosine functions, such that  $\text{cn}(x, 0) = \cos(x)$  and  $\text{cn}(x, 1) = \text{sech}(x)$ ,<sup>23</sup>

$$\phi(\xi) = a_0 + a_1 \text{cn}(\xi),$$

then we get [58]

$$\psi_3(x, t) = \mp m \sqrt{\frac{1}{V(w)}} \text{cn}(x - kt) e^{i[kx - \frac{1}{2}t(1-2m^2+k^2)]}, \quad \text{for } m \in [0, 1); \quad (16)$$

$$\psi_4(x, t) = \mp \sqrt{\frac{1}{V(w)}} \text{sech}(x - kt) e^{i[kx - \frac{1}{2}t(k^2-1)]}, \quad \text{for } m = 1, \quad (17)$$

where (16) defines the general solution, while (17) defines the *crowd envelope solitary-wave* (or, ‘bright soliton’) solution of the crowd NLS equation (1).

In all four solution expressions (14), (15), (16) and (17), the adaptive crowd potential  $V(w)$  is yet to be calculated using either unsupervised Hebbian learning, or supervised Levenberg–Marquardt algorithm (see, e.g. [11]). In this way, the NLS equation (1) becomes a *quantum neural network* [10]. Any kind of numerical analysis can be easily performed using above closed-form crowd solutions  $\psi_i(x, t)$  ( $i = 1, \dots, 4$ ) as initial conditions.

In addition, two new wave-solutions of the crowd NLS equation (1) have been recently provided in [63], in the form of rogue waves,<sup>24</sup> using the deformed Darboux transformation method developed in [66]:

1. The *one-rogon* crowd solution:

$$\psi_{1\text{rogon}}(x, t) = \alpha \sqrt{\frac{1}{2V}} \left[ 1 - \frac{4(1 + \alpha^2 t)}{1 + 2\alpha^2(x - kt)^2 + \sigma^2 \alpha^4 t^2} \right] e^{i[kx + 1/2(\alpha^2 - k^2)t]}, \quad V > 0, \quad (18)$$

where  $\alpha$  and  $k$  denote the crowd scaling and gauge.

2. The *two-rogon* crowd solution:

$$\psi_{2\text{rogon}}(x, t) = \alpha \sqrt{\frac{1}{2V}} \left[ 1 + \frac{P_2(x, t) + iQ_2(x, t)}{R_2(x, t)} \right] e^{i[kx + 1/2(\alpha^2 - k^2)t]}, \quad V > 0, \quad (19)$$

where  $P_2, Q_2, R_2$  are certain polynomial functions of  $x$  and  $t$ .

Both rogon crowd solutions can be easily made adaptive by introducing a set of ‘synaptic weights’ for nonlinear data fitting, in the same way as before.

<sup>23</sup>A closely related solution of an anharmonic oscillator ODE:

$$\phi''(s) + \phi(s) + \phi^3(s) = 0$$

is given by

$$\phi(s) = \sqrt{\frac{2m}{1-2m}} \text{cn} \left( \sqrt{1 + \frac{2m}{1-2m}} s, m \right).$$

<sup>24</sup>Rogue waves are also known as *freak waves*, *monster waves*, *killer waves*, *giant waves* and *extreme waves*. They are found in various media, including optical fibers [64]. The basic rogue wave solution was first presented by Peregrine [65] to describe the phenomenon known as *Peregrine soliton* (or *Peregrine breather*).

## 4.2 Collision of Two Crowds

Next, a bidirectional quantum neural network resembling the strong crowd coupling model (3) has been formulated in [58] as a self-organized system of two coupled NLS equations:

$$\text{Red NLS : } i\partial_t\sigma = -\frac{1}{2}\partial_{xx}\sigma + V(w)(|\sigma|^2 + |\psi|^2)\sigma, \quad (20)$$

$$\text{Blue NLS : } i\partial_t\psi = -\frac{1}{2}\partial_{xx}\psi + V(w)(|\sigma|^2 + |\psi|^2)\psi. \quad (21)$$

In this coupled model, the  $\sigma$ -NLS (20) governs the  $(x, t)$ -evolution of the red crowd, which plays the role of a nonlinear coefficient in the blue crowd (21); the  $\psi$ -NLS (21) defines the  $(x, t)$ -evolution of the blue crowd, which plays the role of a nonlinear coefficient in the red crowd (20). The purpose of this coupling is to generate the *crowd leverage effect* (similar to stock leverage effect in which stock volatility is (negatively) correlated to stock returns. This bidirectional associative memory effectively performs quantum neural computation [10], by giving a spatiotemporal and quantum generalization of Kosko's BAM family of neural networks [67, 68]. In addition, the shock-wave and solitary-wave nature of the coupled NLS equations may describe brain-like effects frequently occurring in crowd dynamics: propagation, reflection and collision of shock and solitary waves (see [59]).

The coupled crowd NLS-system (20)–(21), without an embedded  $w$ -learning (i.e., for constant  $V$ ), actually defines the well-known *Manakov system*,<sup>25</sup> proven by S. Manakov in 1973 [69] to be completely integrable, by the existence of infinite number of involutive integrals of motion. Manakov's own method was based on the *Lax pair representation*.<sup>26</sup> It admits both 'bright' and 'dark' soliton solutions. The simplest solution of (20)–(21), the so-called *Manakov bright 2-soliton* (see Figure 5), has the form resembling that of the sech-solution (17) (see [72, 73, 74, 75, 76, 77, 78]), and is formally defined by:

$$\boldsymbol{\psi}_{\text{sol}}(x, t) = 2b \mathbf{c} \operatorname{sech}[2b(x + 4at)] e^{-2i(2a^2t + ax - 2b^2t)}, \quad (23)$$

where  $\boldsymbol{\psi}_{\text{sol}}(x, t) = \begin{pmatrix} \sigma(x, t) \\ \psi(x, t) \end{pmatrix}$ ,  $\mathbf{c} = (c_1, c_2)^T$  is a unit vector such that  $|c_1|^2 + |c_2|^2 = 1$ . Real-valued parameters  $a$  and  $b$  are some simple functions of  $(V, k)$ , which can be determined by the Levenberg–Marquardt algorithm.

<sup>25</sup>Manakov system has been used to describe the interaction between wave packets in dispersive conservative media, and also the interaction between orthogonally polarized components in nonlinear optical fibres (see, e.g. [70, 71] and references therein).

<sup>26</sup>The Manakov system (20)–(21) has the following Lax pair [79] representation:

$$\begin{aligned} \partial_x \phi &= M\phi \quad \text{and} \quad \partial_t \phi = B\phi, \quad \text{or} \quad \partial_x B - \partial_t M = [M, B], \quad \text{with} \\ M(\lambda) &= \begin{pmatrix} -i\lambda & \psi_1 & \psi_2 \\ -\psi_1 & i\lambda & 0 \\ -\psi_2 & 0 & i\lambda \end{pmatrix} \quad \text{and} \\ B(\lambda) &= -i \begin{pmatrix} 2\lambda^2 - |\psi_1|^2 - |\psi_2|^2 & 2i\psi_1\lambda - \partial_x \psi_1 & 2i\psi_2\lambda - \partial_x \psi_2 \\ -2i\psi_1^* \lambda - \partial_x \psi_1^* & -2\lambda^2 + |\psi_1|^2 & \psi_1^* \psi_2 \\ -2i\psi_2^* \lambda - \partial_x \psi_2^* & \psi_1 \psi_2^* & -2\lambda^2 + |\psi_2|^2 \end{pmatrix}. \end{aligned} \quad (22)$$

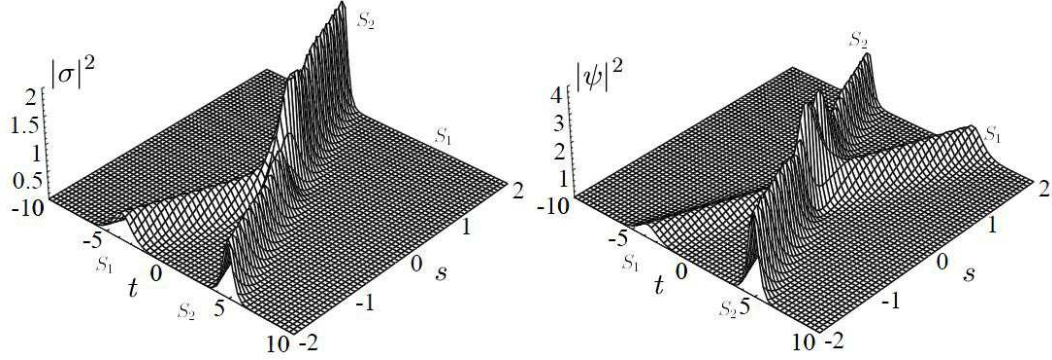


Figure 5: Hypothetical crowd–collision scenario of the Manakov 2–soliton (23). Due to symmetry of the Manakov system, the two crowds ( $\psi$  and  $\sigma$ ) can exchange their roles.

### 4.3 Quantum Linear Crowd Waves

In the case of very weak crowd heat potential  $V(w) \ll 1$ , we have  $V(\psi) \rightarrow 0$ , and therefore equation (1) can be approximated by a quantum-like *crowd wave packet*. It is defined by a continuous superposition of *de Broglie’s plane waves*, ‘physically’ associated with a free quantum particle of unit mass. This linear wave packet, given by the time-dependent complex-valued wave function  $\psi = \psi(x, t)$ , is a solution of the *linear Schrödinger equation* with zero potential energy and the *crowd Hamiltonian operator*  $\hat{H}$ . This equation can be written as:

$$i\partial_t\psi = \hat{H}\psi, \quad \text{where} \quad \hat{H} = -\frac{1}{2}\partial_{xx}. \quad (24)$$

Thus, we consider the  $\psi$ –function describing a single de Broglie’s plane wave, with the wave number  $k$ , linear momentum  $p = k$ , wavelength  $\lambda_k = 2\pi/k$ , angular frequency  $\omega_k = k^2/2$ , and oscillation period  $T_k = 2\pi/\omega_k = 4\pi/k^2$ . It is defined by (compare with [80, 81, 82])

$$\psi_k(x, t) = Ae^{i(kx - \omega_k t)} = Ae^{i(kx - \frac{k^2}{2}t)} = A \cos(kx - \frac{k^2}{2}t) + Ai \sin(kx - \frac{k^2}{2}t), \quad (25)$$

where  $A$  is the amplitude of the wave, the angle  $(kx - \omega_k t) = (kx - \frac{k^2}{2}t)$  represents the phase of the wave  $\psi_k$  with the *crowd phase velocity*:  $v_k = \omega_k/k = k/2$ .

The space-time wave function  $\psi(x, t)$  that satisfies the linear Schrödinger equation (24) can be decomposed (using Fourier’s separation of variables) into the spatial part  $\phi(x)$  and the temporal part  $e^{-i\omega t}$  as:

$$\psi(x, t) = \phi(x) e^{-i\omega t} = \phi(x) e^{-iEt} = \phi(x) e^{-\frac{1}{2}k^2 t},$$

where Planck’s *energy quantum* of the *crowd wave*  $\psi_k$  is given by:  $E_k = \omega_k = \frac{1}{2}k^2$ .

The spatial part, representing *stationary* (or, *amplitude*) *wave function*,  $\phi(x) = Ae^{ikx}$ , satisfies the *crowd harmonic oscillator*, which can be formulated in several equivalent forms:

$$\phi'' + k^2\phi = 0, \quad \phi'' + \left(\frac{\omega_k}{v_k}\right)^2\phi = 0, \quad \phi'' + 2E_k\phi = 0. \quad (26)$$

From the plane-wave expressions (25) we have:  $\psi_k(x, t) = Ae^{i(px - E_k t)}$  – for the wave going to the ‘right’ and  $\psi_k(x, t) = Ae^{-i(px + E_k t)}$  – for the wave going to the ‘left’.

The general solution to (24) is formulated as a linear combination of de Broglie’s planar waves (25), comprising the crowd wave-packet:

$$\psi(x, t) = \sum_{i=0}^n c_i \psi_{k_i}(x, t), \quad (\text{with } n \in \mathbb{N}). \quad (27)$$

Its absolute square,  $|\psi(x, t)|^2$ , represents crowd’s probability density function at a time  $t$ .

The *crowd group velocity* is given by:  $v_g = d\omega_k/dk$ . It is related to the crowd phase velocity  $v_k$ :  $v_g = v_k - \lambda_k dv_k/d\lambda_k$ . Closely related is the *center* of the crowd wave-packet (the point of maximum crowd amplitude), given by:  $x = td\omega_k/dk$ .

The following quantum-motivated assertions can be stated:

1. The total energy  $E$  of an crowd wave-packet is (in the case of similar plane waves) given by Planck’s superposition of the energies  $E_k$  of  $n$  individual agents’ waves:  $E = n\omega_k = \frac{n}{2}k^2$ , where  $L = n$  denotes the *angular momentum* of the crowd wave-packet, representing the shift between its growth and decay, and *vice versa*.
2. The average energy  $\langle E \rangle$  of an crowd wave-packet is given by Boltzmann’s partition function:

$$\langle E \rangle = \frac{\sum_{n=0}^{\infty} n E_k e^{-\frac{n E_k}{bT}}}{\sum_{n=0}^{\infty} e^{-\frac{n E_k}{bT}}} = \frac{E_k}{e^{\frac{E_k}{bT}} - 1},$$

where  $b$  is the Boltzmann-like kinetic constant and  $T$  is the crowd ‘temperature’.

3. The energy form of the Schrödinger equation (24) reads:  $E\psi = i\partial_t\psi$ .
4. The eigenvalue equation for the crowd Hamiltonian operator  $\hat{H}$  is the *stationary Schrödinger equation*:

$$\hat{H}\phi(x) = E\phi(x), \quad \text{or} \quad E\phi(x) = -\frac{1}{2}\partial_{xx}\phi(x),$$

which is just another form of the harmonic oscillator (26). It has oscillatory solutions of the form:

$$\phi_E(x) = c_1 e^{i\sqrt{2E_k}x} + c_2 e^{-i\sqrt{2E_k}x},$$

called *energy eigen-states* with energies  $E_k$  and denoted by:  $\hat{H}\phi_E(x) = E_k\phi_E(x)$ .

Now, given some initial crowd wave function,  $\psi(x, 0) = \psi_0(x)$ , a solution to the initial-value problem for the linear Schrödinger equation (24) is, in terms of the pair of Fourier transforms ( $\mathcal{F}, \mathcal{F}^{-1}$ ), given by (see [81])

$$\psi(x, t) = \mathcal{F}^{-1} [e^{-i\omega t} \mathcal{F}(\psi_0)] = \mathcal{F}^{-1} \left[ e^{-i\frac{k^2}{2}t} \mathcal{F}(\psi_0) \right]. \quad (28)$$

For example (see [81]), suppose we have an initial crowd wave-function at time  $t = 0$  given by the complex-valued Gaussian function:

$$\psi(x, 0) = e^{-ax^2/2} e^{ikx},$$

where  $a$  is the width of the Gaussian, while  $p$  is the average momentum of the wave. Its Fourier transform,  $\hat{\psi}_0(k) = \mathcal{F}[\psi(x, 0)]$ , is given by

$$\hat{\psi}_0(k) = \frac{e^{-\frac{(k-p)^2}{2a}}}{\sqrt{a}}.$$

The solution at time  $t$  of the initial value problem is given by

$$\psi(x, t) = \frac{1}{\sqrt{2\pi a}} \int_{-\infty}^{+\infty} e^{i(kx - \frac{k^2}{2}t)} e^{-\frac{a(k-p)^2}{2a}} dk,$$

which, after some algebra becomes

$$\psi(x, t) = \frac{\exp(-\frac{ax^2 - 2ixp + ip^2t}{2(1+iat)})}{\sqrt{1+iat}}, \quad (\text{with } p = k).$$

As a simpler example,<sup>27</sup> if we have an initial crowd wave-function given by the real-valued Gaussian function,

$$\psi(x, 0) = \frac{e^{-x^2/2}}{\sqrt[4]{\pi}},$$

the solution of (24) is given by the complex-valued  $\psi$ -function,

$$\psi(x, t) = \frac{\exp(-\frac{x^2}{2(1+it)})}{\sqrt[4]{\pi}\sqrt{1+it}}.$$

From (28) it follows that a stationary crowd wave-packet is given by:

$$\phi(x) = \frac{1}{\sqrt{2\pi}} \int_{-\infty}^{+\infty} e^{ikx} \hat{\psi}(k) dk, \quad \text{where} \quad \hat{\psi}(k) = \mathcal{F}[\phi(x)].$$

As  $|\phi(x)|^2$  is the stationary crowd PDF, we can calculate the *crowd expectation values* and the wave number of the whole crowd wave-packet, consisting of  $n$  measured plane waves, as:

$$\langle x \rangle = \int_{-\infty}^{+\infty} x |\phi(x)|^2 dx \quad \text{and} \quad \langle k \rangle = \int_{-\infty}^{+\infty} k |\hat{\psi}(k)|^2 dk. \quad (29)$$

The recordings of  $n$  individual crowd plane waves (25) will be scattered around the mean values (29). The width of the distribution of the recorded  $x$ - and  $k$ -values are uncertainties  $\Delta x$  and  $\Delta k$ , respectively. They satisfy the Heisenberg-type uncertainty relation:

$$\Delta x \Delta k \geq \frac{n}{2},$$

---

<sup>27</sup>An example of a more general Gaussian wave-packet solution of (24) is given by:

$$\psi(x, t) = \sqrt{\frac{\sqrt{a/\pi}}{1+iat}} \exp\left(\frac{-\frac{1}{2}a(s-s_0)^2 - \frac{1}{2}p_0^2t + ip_0(s-s_0)}{1+iat}\right),$$

where  $s_0, p_0$  are initial stock-price and average momentum, while  $a$  is the width of the Gaussian. At time  $t = 0$  the 'particle' is at rest around  $s = 0$ , its average momentum  $p_0 = 0$ . The wave function spreads with time while its maximum decreases and stays put at the origin. At time  $-t$  the wave packet is the complex-conjugate of the wave-packet at time  $t$ .

which imply the similar relation for the total crowd energy and time:

$$\Delta E \Delta t \geq \frac{n}{2}.$$

## 5 Conclusion

In this paper we gave a formal mathematical and physical description of nonlinear phenomena in dynamics of human crowds. While Helbing discovered a phenomenon of crowd turbulence (see Introduction), we felt that equally important would be to model related but different crowd phenomena, such as solitons, rogue waves and shock waves. Our proposal, including both classical and quantum description of crowd turbulence, as well as both nonlinear and quantum crowd waves, provides a new basis for studying all these nonlinear phenomena in crowds.

## 6 Appendix: Basic Lie Algebra Mechanics

A *manifold*  $M$  is a topological space that on a small scale (locally) resembles the Euclidean space. Manifolds are usually endowed with a differentiable structure that allows one to do calculus and differential equations, as well as a *Riemannian metric* that allows one to measure distances and angles. For example, Riemannian manifolds are the configuration spaces for Lagrangian mechanics, while symplectic manifolds are the phase spaces in the Hamiltonian mechanics. A *diffeomorphism* is an invertible function that maps one smooth (differentiable) manifold to another, such that both the function and its inverse are smooth.

A *Lie group*  $G$  is a smooth manifold  $M$  that has at the same time a group  $G$ -structure consistent with its manifold  $M$ -structure in the sense that *group multiplication*  $\mu : G \times G \rightarrow G$ ,  $(g, h) \mapsto gh$  and the *group inversion*  $\nu : G \rightarrow G$ ,  $g \mapsto g^{-1}$  are smooth maps. A point  $e \in G$  is called the group identity element.

A Lie group can *act* on a smooth manifold  $M$  by moving the points of  $M$ , denoted by  $G \times M \rightarrow M$ . Group action on a manifold defines the *orbit* of a point  $m$  on a manifold  $M$ , which is the set of points on  $M$  to which  $m$  can be moved by the elements of a Lie group  $G$ . The orbit of a point  $m$  is denoted by  $Gm = \{g \cdot m | g \in G\}$ .

Let  $G$  be a real Lie group. Its *Lie algebra*  $\mathfrak{g}$  is the tangent space  $TG_e$  to the group  $G$  at the identity  $e$  provided with the *Lie bracket (commutator)* operation  $[X, Y]$ , which is bilinear, skew-symmetric, and satisfies the *Jacobi identity* (for any three vector fields  $X, Y, Z \in \mathfrak{g}$ ):

$$[[X, Y], Z] = [X, [Y, Z]] - [X, [Y, Z]].$$

Note that in Hamiltonian mechanics, Jacobi identity is satisfied by Poisson brackets, while in quantum mechanics it is satisfied by operator commutators.

For example,  $G = SO(3)$  is the group of rotations of 3D Euclidean space, i.e. the configuration space of a rigid body fixed at a point. A motion of the body is then described by a curve  $g = g(t)$  in the group  $SO(3)$ . Its Lie algebra  $\mathfrak{g} = \mathfrak{so}(3)$  is the 3D vector space of angular velocities of all possible rotations. The commutator in this algebra is the usual vector (cross) product.

A Lie group  $G$  acts on itself by left and right translations: every element  $g \in G$  defines diffeomorphisms of the group onto itself (for every  $h \in G$ ):

$$L_g : G \rightarrow G, \quad L_g h = gh; \quad R_g : G \rightarrow G, \quad R_g h = hg.$$

The induced maps of the tangent spaces are denoted by:

$$L_{g*} : TG_h \rightarrow TG_{gh}, \quad R_{g*} : TG_h \rightarrow TG_{hg}.$$

The diffeomorphism  $R_{g^{-1}}L_g$  is an inner automorphism of the group  $G$ . It leaves the group identity  $e$  fixed. Its derivative at the identity  $e$  is a linear map from the Lie algebra  $\mathfrak{g}$  to itself:

$$Ad_g : \mathfrak{g} \rightarrow \mathfrak{g}, \quad Ad_g(R_{g^{-1}}L_g)_{*e}$$

is called the *adjoint representation* of the Lie group  $G$ .

Referring to the previous example, a rotation velocity  $\dot{g}$  of the rigid body (fixed at a point) is a tangent vector to the Lie group  $G = SO(3)$  at the point  $g \in G$ . To get the angular velocity, we must carry this vector to the tangent space  $TG_e$  of the group at the identity, i.e. to its Lie algebra  $\mathfrak{g} = \mathfrak{so}(3)$ . This can be done in two ways: by left and right translation,  $L_g$  and  $R_g$ . As a result, we obtain two different vector fields in the Lie algebra  $\mathfrak{so}(3)$  :

$$\omega_c = L_{g^{-1}*}\dot{g} \in \mathfrak{so}(3) \quad \text{and} \quad \omega_x = R_{g^{-1}*}\dot{g} \in \mathfrak{so}(3),$$

which are called the ‘angular velocity in the body’ and the ‘angular velocity in space,’ respectively.

Now, left and right translations induce operators on the cotangent space  $T^*G_g$  dual to  $L_{g*}$  and  $R_{g*}$ , denoted by (for every  $h \in G$ ):

$$L_g^* : T^*G_{gh} \rightarrow T^*G_h, \quad R_g^* : T^*G_{hg} \rightarrow T^*G_h.$$

The transpose operators  $Ad_g^* : \mathfrak{g} \rightarrow \mathfrak{g}$  satisfy the relations  $Ad_{gh}^* = Ad_h^*Ad_g^*$  (for every  $g, h \in G$ ) and constitute the *co-adjoint representation* of the Lie group  $G$ . The co-adjoint representation plays an important role in all questions related to (left) invariant metrics on the Lie group. According to A. Kirillov, the orbit of any vector field  $X$  in a Lie algebra  $\mathfrak{g}$  in a co-adjoint representation  $Ad_g^*$  is itself a symplectic manifold and therefore a phase space for a Hamiltonian mechanical system.

A Riemannian metric on a Lie group  $G$  is called left-invariant if it is preserved by all left translations  $L_g$ , i.e., if the derivative of left translation carries every vector to a vector of the same length. Similarly, a vector field  $X$  on  $G$  is called left-invariant if (for every  $g \in G$ )  $L_g^*X = X$ .

Again referring to the previous example of the rigid body, the dual space  $\mathfrak{g}^*$  to the Lie algebra  $\mathfrak{g} = \mathfrak{so}(3)$  is the space of angular momenta  $\boldsymbol{\pi}$ . The kinetic energy  $T$  of a body is determined by the vector field of angular velocity in the body and does not depend on the position of the body in space. Therefore, kinetic energy gives a left-invariant Riemannian metric on the rotation group  $G = SO(3)$ .

## References

- [1] V. Ivancevic, D. Reid, E. Aidman, Crowd behavior dynamics: entropic path-integral model. *Nonl. Dyn.* **59**, 351-373, (2010)
- [2] V. Ivancevic, D. Reid, Crowd behavior dynamics: entropic path-integral model. *Nonl. Dyn. Entropic geometry of crowd dynamics. A Chapter in Nonlinear Dynamics* (T. Evancs, Ed.), Intech, Vienna, (2010)



- [3] V. Ivancevic, D. Reid, Geometrical and Topological Duality in Crowd Dynamics. *Int. J. Biomath.* **3**(4), (2010), 493–507.
- [4] V. Ivancevic, D. Reid, Dynamics of Confined Crowds Modelled using Entropic Stochastic Resonance and Quantum Neural Networks. *Int. J. Intel. Defence Sup. Sys.* **2**(4), 269-289, (2009)
- [5] Helbing, D., Molnar, P., Social force model for pedestrian dynamics. *Phys. Rev. E* 1995, **51**(5), 4282–4286.
- [6] Helbing, D., Farkas, I., Vicsek, T. Simulating dynamical features of escape panic. *Nature* **407**, (2000), 487–490.
- [7] Helbing, D., Johansson, A., Mathiesen, J., Jensen, M.H., Hansen, A. Analytical approach to continuous and intermittent bottleneck flows. *Phys. Rev. Lett.* **97**, (2006), 168001.
- [8] Helbing, D., Johansson, A., Zein Al-Abideen, H. The Dynamics of Crowd Disasters: An Empirical Study. *Phys. Rev. E* **75**, (2007), 046109.
- [9] Johansson, A., Helbing, D., Z. Al-Abideen, H., Al-Bosta, S. From Crowd Dynamics to Crowd Safety: A Video-Based Analysis. *Adv. Com. Sys.* **11**(4), (2008), 497–527.
- [10] V. Ivancevic, T. Ivancevic, *Quantum Neural Computation*, Springer, (2009)
- [11] Ivancevic, V., Ivancevic, T., *Neuro-Fuzzy Associative Machinery for Comprehensive Brain and Cognition Modelling*. Springer, Berlin, (2007)
- [12] Tao, T., *Nonlinear dispersive equations: local and global analysis*, CBMS regional series in mathematics, (2006)
- [13] Arnold V.I., *Mathematical Methods of Classical Mechanics* (2ed.), Springer, (1989)
- [14] Arnold V.I., Khezin B., *Topological Methods in Hydrodynamics*, Springer, (1998)
- [15] Ivancevic, V., Ivancevic, T., *Geometrical Dynamics of Complex Systems: A Unified Modelling Approach to Physics Control Biomechanics Neurodynamics and Psycho-Socio-Economical Dynamics*. Springer: Dordrecht, 2006.
- [16] Ivancevic, V., Ivancevic, T., *Applied Differential Geometry: A Modern Introduction*. World Scientific: Singapore, 2007.
- [17] Ruelle, D., Takens, F., On the nature of turbulence, *Comm. Math. Phys.* **20**(2), (1971), 167-192; *Comm. Math. Phys.* **23**(3), (1971), 343-344.
- [KK01] Kawahara, G., Kida, S.: Periodic motion embedded in plane Couette turbulence: regeneration cycle and burst. *J. Fluid Mech.* **449**, 291–300, (2001)
- [18] Kirchhoff, G.R., *Vorlesungen über mathematische Physik. Mechanik*, Leipzig, Teubner, (1876), 466 pp.
- [19] Tsubota, M. Quantized vortices in superfluid helium and Bose-Einstein condensates. *J. Physics: Conf. Ser.* **31**, 88–94, (2006)

- [20] Tsubota, M., Kasamatsu, K, Kobayashi, M. Quantized vortices in superfluid helium and atomic Bose-Einstein condensates. arXiv: cond-mat.quant-gas 1004.5458v2, (2010)
- [21] Pitaevskii, L. and Stringari, S. (2003). Bose-Einstein Condensation. Oxford University Press, Oxford.
- [22] Kapitza, P., Viscosity of liquid helium below the  $\lambda$  point. Nature **141**, (1938), 74.
- [23] Allen, J.F., Misener, A.D., Flow of liquid helium II. Nature, **141**, (1938), 75.
- [24] Landau, L. (1941). The theory of superfluidity of helium II. J. Phys. U.S.S.R. **5**, 71-90.
- [25] Tisza, L. (1938). Transport phenomena in helium II. Nature, 141, 913.
- [26] Gorter, C J., Mellink, J.H. (1949). On the irreversible processes in liquid helium II. Physica, **15**, 285-304.
- [27] London, F. (1938). On the Bose-Einstein condensation. Phys. Rev. **54**, 947-954.
- [28] Onsager, L. (1949). Nuovo Cimento Suppl. **6**, 249-250.
- [29] Feynman, R.P. (1955). Application of quantum mechanics to liquid helium. Progress in Low Temperature Physics Vol.1(Gorter, C. J. ed.). Amsterdam. North-Holland, 17-53.
- [30] Hall, H. E. and Vinen, W. F. (1956). The rotation of liquid helium II I. Experiments on the propagation of second sound in uniformly rotating helium II. Proc. Roy. Soc. London, A **238**, 204-214.
- [31] Hall, H. E. and Vinen, W. F. (1956). The rotation of liquid helium II II. The theory of mutual friction in uniformly rotating helium II. Proc. Roy. Soc. London, A **238**, 215-234.
- [32] Vinen, W.F. (1957). Mutual friction in a heat current in liquid helium II I. Experiments on steady heat currents, Proc. Roy. Soc. London, A **240**, 114-127.
- [33] Vinen, W. F. (1957). Mutual friction in a heat current in liquid helium II. II. Experiments on transient effects. Proc. Roy. Soc. London, A **240**, 128-143.
- [34] Vinen, W. F. (1957). Mutual friction in a heat current in liquid helium II III. Theory of mutual friction. Proc. Roy. Soc. London, A **242**, 493-515.
- [35] Vinen, W. F. (1957). Mutual friction in a heat current in liquid helium II IV. Critical heat currents in wide channels. Proc. Roy. Soc. London, A **243**, 400-413.
- [36] Vinen, W. F. (1961). The detection of single quanta circulation in liquid helium II. Proc. Roy. Soc. London, A **260**, 218-236.
- [37] Tough, J. T. (1982). Superfluid turbulence. Progress in Low Temperature Physics Vol. 8 (Gorter, C. J. ed.). Amsterdam. North-Holland, 133-220.
- [38] Schwarz, K. W. (1985). Three-dimensional vortex dynamics in superfluid  $^4\text{He}$ : Line-line and line-boundary interactions. Phys. Rev. B **31**, 5782-5803.

- [39] Schwarz, K. W. (1988). Three-dimensional vortex dynamics in superfluid  $^4\text{He}$ : Homogeneous superfluid turbulence. *Phys. Rev. B* **38**, 2398-2417.
- [40] G.A. Williams and R.E. Packard, Photographs of quantized vortex lines in rotating He II, *Phys. Rev. Lett.* **33** (1974), 280–283.
- [41] E.J. Yarmchuck and R.E. Packard, Photographic studies of quantized vortex lines, *J. Low Temp. Phys.* **46** (1982), 479–515.
- [42] M.R. Matthews, B.P. Anderson, P. C. Haljan, D. S. Hall, C. E. Wieman, and E. A. Cornell, Vortices in a Bose-Einstein condensate, *Phys. Rev. Lett.* **83** (1999), 2498–2501.
- [43] J.R. Abo-Shaeer, C. Raman, J. M. Vogels, and W. Ketterle, Observation of vortex lattices in Bose-Einstein condensates, *Science* **292** (2001), 476–479.
- [44] K.W. Madison, F. Chevy, W. Whllleben, and J. Dalibard, Vortex formation in a stirred Bose-Einstein condensate, *Phys. Rev. Lett.* **84** (2000), 806–809.
- [45] K.W. Madison, F. Chevy, W. Whllleben, and J. Dalibard, Stationary states of a rotating Bose-Einstein condensate: Routes to vortex nucleation, *Phys. Rev. Lett.* **86** (2001), 4443–4446.
- [46] M. Tsubota, K. Kasamatsu, and M. Ueda, Vortex lattice formation in a rotating Bose-Einstein condensate, *Phys. Rev. A* **65** (2002), 023603.
- [47] K. Kasamatsu, M. Tsubota, and M. Ueda, Nonlinear dynamics of vortex lattice formation in a rotating Bose-Einstein condensate, *Phys. Rev. A* **67** (2003), 033610.
- [48] K. Kasamatsu, M. Machida, N. Sasa and M. Tsubota, Three-dimensional dynamics of vortex-lattice formation in Bose-Einstein condensate *Phys. Rev. A* **71** (2005), 063616.
- [49] U. Frisch, *Turbulence*, Cambridge University Press, Cambridge, 1995.
- [50] A.N. Kolmogorov, The local structure of turbulence in incompressible viscous fluid for very large Reynolds number, *Dokl. Akad. Nauk SSSR* **30** (1941), 299-303 [reprinted in *Proc. Roy. Soc. A* **434** (1991), 9-13].
- [51] A.N. Kolmogorov, On degeneration (decay) of isotropic turbulence in an incompressible viscous liquid, *Dokl. Akad. Nauk SSSR* **31** (1941), 538-540 [reprinted in *Proc. Roy. Soc. A* **434** (1991), 15-17].
- [52] M. Leadbeater, T. Winiecki, D. C. Samuels, C. F. Barenghi, and C. S. Adams, Sound emission due to superfluid vortex reconnections, *Phys. Rev. Lett.* **86** (2001), 1410-1413.
- [53] S. Ogawa, M. Tsubota, and Y. Hattori, Study of reconnection and acoustic emission of quantized vortices in superfluid by the numerical analysis of the Gross-Pitaevskii equation, *J. Phys. Soc. Jpn.* **71** (2002), 813-821.
- [54] M. Kobayashi and M. Tsubota, Kolmogorov spectrum of superfluid turbulence: Numerical analysis of the Gross-Pitaevskii equation with a small-scale dissipation, *Phys. Rev. Lett.* **94** (2005), 065302.

- [55] M. Kobayashi and M. Tsubota, Kolmogorov spectrum of quantum turbulence, *J. Phys. Soc. Jpn.* **74** (2005), 3248-3258.
- [56] C. Nore, M. Abid, and M. E. Brachet, Kolmogorov turbulence in low-temperature superflows, *Phys. Rev. Lett.* **78** (1997), 3296-3299.
- [57] C. Nore, M. Abid, and M. E. Brachet, Decaying Kolmogorov turbulence in a model of superflow, *Phys. Fluids* **9** (1997), 2644-2669.
- [58] V. Ivancevic, Adaptive-Wave Alternative for the Black-Scholes Option Pricing Model, *Cogn. Comput.* **2** (2010), 17–30.
- [59] S.-H. Hanm, I.G. Koh, Stability of neural networks and solitons of field theory. *Phys. Rev. E* **60**, 7608–7611, (1999)
- [60] S. Liu, Z. Fu, S. Liu, Q. Zhao, Jacobi elliptic function expansion method and periodic wave solutions of nonlinear wave equations. *Phys. Let. A* **289**, 69–74, (2001)
- [61] G-T. Liu, T-Y. Fan, New applications of developed Jacobi elliptic function expansion methods. *Phys. Let. A* **345**, 161–166, (2005)
- [62] M. Abramowitz, I.A. Stegun, (Eds): *Jacobian Elliptic Functions and Theta Functions*. Chapter 16 in *Handbook of Mathematical Functions with Formulas, Graphs, and Mathematical Tables* (9th ed). Dover, New York, 567-581, (1972)
- [63] Z. Yan, Financial rogue waves (in press) arXiv.q-fin.PR:0911.4259; *Optical Rogue Waves (Rogons)*, Wolfram Demonstration Project, (2009)
- [64] D.R. Solli, C. Ropers, P. Koonath, B. Jalali, Optical Rogue Waves, *Nature* **450**, 1054–1057, (2007)
- [65] D.H. Peregrine, *Water Waves, Nonlinear Schrödinger Equations and Their Solutions*, *J. Austral. Math. Soc. Ser. B* **25**, 16–43, (1983)
- [66] N. Akhmediev, A. Ankiewicz, M. Taki, Waves That Appear from Nowhere and Disappear without a Trace, *Phys. Lett. A* **373**(6), 675–678, (2009); N. Akhmediev, A. Ankiewicz, J. M. Soto-Crespo, Rogue Waves and Rational Solutions of the Nonlinear Schrödinger Equation, *Phys. Rev. E* **80**(2), 026601, (2009)
- [67] B. Kosko, Bidirectional Associative Memory. *IEEE Trans. Sys. Man Cyb.* **18**, 49–60, (1988)
- [68] B. Kosko, *Neural Networks, Fuzzy Systems, A Dynamical Systems Approach to Machine Intelligence*. Prentice–Hall, New York, (1992)
- [69] S.V. Manakov, On the theory of two-dimensional stationary self-focusing of electromagnetic waves. (in Russian) *Zh. Eksp. Teor. Fiz.* **65**, (1973), 505-516; (translated into English) *Sov. Phys. JETP* **38**, 248–253, (1974)
- [70] M. Haelterman, A.P. Sheppard, Bifurcation phenomena and multiple soliton bound states in isotropic Kerr media. *Phys. Rev. E* **49**, 3376-3381, (1994)

- [71] J. Yang, Classification of the solitary wave in coupled nonlinear Schrödinger equations. *Physica D* **108**, 92-112, (1997)
- [72] D.J. Benney, A.C. Newell, The propagation of nonlinear wave envelopes. *J. Math. Phys.* **46**, 133-139, (1967)
- [73] V.E. Zakharov, S.V. Manakov, S.P. Novikov, L.P. Pitaevskii, *Soliton theory: inverse scattering method*. Nauka, Moscow, (1980)
- [74] A. Hasegawa, Y. Kodama, *Solitons in Optical Communications*. Clarendon, Oxford, (1995)
- [75] R. Radhakrishnan, M. Lakshmanan, J. Hietarinta, Inelastic collision and switching of coupled bright solitons in optical fibers. *Phys. Rev. E* **56**, 2213, (1997)
- [76] G. Agrawal, *Nonlinear fiber optics* (3rd ed.). Academic Press, San Diego, (2001).
- [77] J. Yang, Interactions of vector solitons. *Phys. Rev. E* **64**, 026607, (2001)
- [78] J. Elgin, V. Enolski, A. Its, Effective integration of the nonlinear vector Schrödinger equation. *Physica D* **225**(22), 127-152, (2007)
- [79] P. Lax, Integrals of nonlinear equations of evolution and solitary waves. *Comm. Pure Applied Math.* **21**, 467-490, (1968)
- [80] D.J. Griffiths, *Introduction to Quantum Mechanics* (2nd ed.), Pearson Educ. Int., (2005)
- [81] B. Thaller, *Visual Quantum Mechanics*, Springer, New York, (2000)
- [82] V. Ivancevic, T. Ivancevic, *Quantum Leap: From Dirac and Feynman, Across the Universe, to Human Body and Mind*. World Scientific, Singapore, (2008)